Sphere-to-Rod Transitions of Nonionic Surfactant Micelles in Aqueous Solution Modeled by Molecular Dynamics Simulations

ARTICLE *in* LANGMUIR · DECEMBER 2011

Impact Factor: 4.46 · DOI: 10.1021/la203055t · Source: PubMed

4 AUTHORS:

Maria Velinova
Sofia University "St. Kliment Ohridski"
9 PUBLICATIONS **55** CITATIONS
SEE PROFILE

Durba Sengupta
CSIR - National Chemical Laboratory, Pune
36 PUBLICATIONS **934** CITATIONS
SEE PROFILE

A. Tadjer
Sofia University "St. Kliment Ohridski"
66 PUBLICATIONS **431** CITATIONS
SEE PROFILE

Siewert J Marrink
University of Groningen
212 PUBLICATIONS **14,165** CITATIONS
SEE PROFILE

Langmuir

ARTICLE

pubs.acs.org/Langmuir

Sphere-to-Rod Transitions of Nonionic Surfactant Micelles in Aqueous Solution Modeled by Molecular Dynamics Simulations

Maria Velinova,[†] Durba Sengupta,[‡] Alia V. Tadjer,*[,†] and Siewert-Jan Marrink[‡]

[†]Laboratory of Quantum and Computational Chemistry, Department of Physical Chemistry, Faculty of Chemistry, University of Sofia, 1 James Bourchier Avenue, 1164 Sofia, Bulgaria

[‡]Groningen Biomolecular Sciences and Biotechnology Institute and Zernike Institute for Advanced Materials, University of Groningen, Nijenborgh 4, 9747 AG Groningen, The Netherlands

Supporting Information

ABSTRACT: Control of the size and agglomeration of micellar systems is important for pharmaceutical applications such as drug delivery. Although shape-related transitions in surfactant solutions are studied experimentally, their molecular mechanisms are still not well understood. In this study, we use coarse-grained molecular dynamics simulations to describe micellar assemblies of pentaethylene glycol monododecyl ether ($C_{12}E_5$) in aqueous solution at different concentrations. The obtained size and aggregation numbers of the aggregates formed are in very good agreement with the available experimental data. Importantly, increase of the concentration leads to a second critical micelle concentration where a transition to rod-like aggregates is observed. This transition is quantified in terms of shape anisotropy, together with a detailed structural analysis of the micelles as a function of aggregation number.

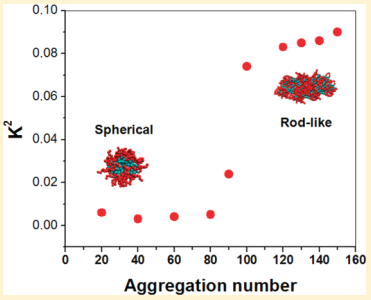

INTRODUCTION

The amphiphilic nature of surfactants makes them prone to their spontaneous aggregation and self-organization in a variety of supramolecular forms such as micelles, vesicles, emulsions, and liquid crystals.[1] The micelle shape in solution can be controlled by different factors including temperature, concentration, additives, and ionic strength. Variation of these parameters may result in modifications of micellar structure and eventually in geometrical transitions. It is demonstrated experimentally that micelles can adopt various shapes: spheres, discs, ellipsoids, or rods, and that at low concentrations of nonionic surfactants the micelles formed are close to spherical. The increase of concentration may lead to two effects:[2,3] either to a growth in the number of spherical aggregates with minor changes of their size or to the registration of a second critical concentration of micellization (CMC) characterizing the transition to rod-like assemblies.

Nonionic surfactants of the alkyl poly(ethylene glycol) type, denoted as C_mE_n, where m is the number of carbons in the alkyl chain and n is the number of glycol units in the poly(ethylene glycol) moiety, are extensively utilized in biochemical investigations as detergents, solubilizers, and emulsifiers.[4] An interesting representative of this class is the compound $C_{12}E_5$,[5] featuring two separate stages of micellization upon rise of concentration and temperature. In the study of Arabadzhieva and coauthors,[6] the surface tension isotherms at 20 °C of aqueous solutions of $C_{12}E_5$ are measured by profile analysis tensiometry. The experiment shows that surfactant solutions from the intermediate concentration range, well beneath CMC, contain amphiphilic nanostructures, which are related to the appearance of a kink and plateau portions in the surface tension isotherm. These are loose aggregates, which contain less surfactant molecules than the regular micelles above CMC. Otto Glatter et al.[7] examine experimentally a $C_{12}E_5$ solution from 3 °C to the cloud temperature ($T_c \approx 28$ °C[8]) with a combination of SANS and viscosity measurements interpreting their data as the formation of rod-like micelles. In essence, they show a sphere-to-rod transition occurring with increase of temperature.

This transition can be explained on the basis of molecular level theory. Ben-Shaul et al.[9] study the grouping of amphiphiles in linear micelles and prove the hypothesis of a second critical micelle concentration (indicating in this case the sphere-to-rod transition) through calculation of the micellar size distributions and average aggregation numbers as a function of the total amphiphile concentration. Furthermore, Daful et al.[10] use a single chain mean field theory (SCMFT) to quantitatively describe the micellization process of the nonionic polyethylene oxide alkyl ether class of surfactants. An explicit but simple microscopic model with only three interaction parameters is shown to be able to reproduce CMCs of a wide range of head and tail surfactant lengths. As expected, the CMC values decrease exponentially with increasing surfactant tail length, whereas they slightly increase with an increase of the head length of the surfactant. However, the SCMFT was found on the whole to overestimate the aggregation numbers and is expected to be sensitive to the details of the model used.

Received: August 5, 2011
Revised: October 4, 2011
Published: October 07, 2011

Phenomenological thermodynamics models, although very powerful to predict many of the properties of nonionic surfactant solutions, do not reveal any details about the mechanism of formation of surfactant aggregates and the micellar structure.[11] Lately, molecular dynamics (MD) simulations have emerged as a powerful tool for investigating the static and dynamic structure of micelles. The advantage of this approach is that time-dependent phenomena become accessible. MD simulations with the CHARMM22 force field are reported[12] for three different spherical aggregates in water solution consisting of the poly(oxyethylene) surfactants, C_{12}, $C_{12}E_0$, and $C_{12}E_3$. The study investigates the structural changes of the aggregate and the conformational modifications of its chains upon increasing the hydrophilicity of the monomers. It is found that the surface of the core region is strongly fluctuating and its thickness is enhanced when the length of the hydrophilic part of the monomers is increased. Other MD simulations[13] have been carried out to study the microscopic properties of a reverse micelle of $C_{12}E_2$ in nonpolar environments. The conformational properties of the surfactant headgroups and the arrangement of water molecules around them are also investigated in detail. It is observed that there is a strong tendency for the core water molecules to form hydrogen-bonded bridged structures between the two adjacent oxyethylene group oxygen atoms. This leads to an exclusive preference for headgroup conformations with gauche C−C bonds.

Although MD simulations provide an atomistic level of insight and are capable of studying the micellar self-assembly process,[14−16] the computational burden prevents these studies from generating equilibrium ensembles except in some cases pertaining to very soluble surfactants.[17] To overcome this limitation and to investigate slower processes, a coarse-grained (CG) level of description is required. By omitting the full atomistic details, processes that are essential to reach equilibrium, such as micellar fusion and fission, and intermicelle monomer exchange, can be simulated.[18−20] On the basis of a CG model, Shinoda et al.[21] have studied the phase behavior of solutions of poly(ethylene glycol) type surfactants, including the micelle forming $C_{12}E_6$. They have shown a transition from micelles to hexagonal and lamellar phases upon increasing surfactant concentration in the range 20−80 wt %.

In the current work, we use the MARTINI CG force field,[22,23] which has been optimized to reproduce phase behavior of a large variety of lipid and surfactant systems. A coarse-grained model of poly(ethylene oxide) (PEO) and poly(ethylene glycol) (PEG) has recently been developed[24] within the framework of MARTINI. The MARTINI force field enables dynamical explorations using larger systems over time scales sufficiently long to capture shape fluctuations and the sphere-to-rod transition of the micelles, as exemplified in the recent study of Sangwai et al.[25] In that study, the transition is observed for cetyltrimethylammonium chloride (CTAC) micelles upon the addition of aromatic salts. In a comparative study of Sanders and Panagiotopoulos,[26] it is concluded that the MARTINI model can reproduce experimental CMCs and aggregation numbers for nonionic surfactants reasonably well. The temperature dependence, however, is shown to be incorrect, a known shortcoming of the CG models. Another interesting study of Lee and Pastor[27] used the MARTINI coarse-grained force field for investigation of the self-assembly of PEG-grafted lipids showing a vesicle−bicelle−micelle transition dependent on the PEG concentration in line with the experimental measurements.

The objective of this study is the investigation of the self-assembly of the nonionic surfactant $C_{12}E_5$ in aqueous solution at different concentrations and clarification of the structure of the formed aggregates. The transition from spherical to rod-like shape of $C_{12}E_5$ micelles is demonstrated, and important molecular details of the mechanism of the transition are outlined.

Table 1. Number of Surfactants (N_{sur}) and CG Water Beads (N_{water}), Linear Size (L) of the Periodic Box, and Weight Mass (w) and Molar (χ) Fraction of the Surfactants in the Modeled Systems[a]

systems	N_{water}	N_{sur}	L [nm]	w [%]	χ [%]
1	31 882	160	16	2.71	0.13
2	48 002	360	18	4.12	0.19
3	59 263	780	19	6.89	0.33
4	60 451	1000	20	8.56	0.41
5	3996	20	8	2.71	0.13
6	7638	40	9	2.73	0.13
7	11 857	60	10	2.72	0.13
8	14 109	80	11	2.7	0.14
9	16 709	100	12	3.2	0.15
10	20 934	120	13	3.2	0.14

[a] Note that a CG water bead represents four real water molecules; w and χ are calculated with respect to the number of real waters.

METHODS AND MODELS

System Setup. To the end of obtaining more in-depth information about the mechanism of self-organization of $C_{12}E_5$, large-scale CGMD simulations of systems corresponding to various concentrations above the CMC (0.064 mM[28]) are performed. All simulations are initiated from random distribution of the molecules in a cubic periodic box. More details of the systems are presented in Table 1 (systems 1−4). The choice of these systems corresponds to the experimental methodologies of investigation of this phenomenon.[29]

For more exhaustive analyses of the structural properties of the micelles, additional simulations are performed of preconstructed spherical micelles containing, respectively, 20, 40, 60, 80, 100, and 120 surfactant molecules in excess of solvent (see Table 1, systems 5−10). These systems are simulated for 1 μs.

All CG-MD simulations are carried out with GROMACS 4.0,[30] using the leapfrog integration algorithm with a time step 10 fs in the NPT ensemble. The pressure and temperature are maintained at 1 bar and 298 K by means of the Berendsen method.[31] The cutoff used for the nonbonding interactions is 1.2 nm, using shifted potentials according to the standard MARTINI protocol.[22,23] The equilibration of the system is monitored through convergence of the potential energy. The analyses are based on the last 2.5 μs of the simulations for systems 1−4, and on the last 900 ns for systems 5−10.

Force Field Details. The MARTINI force field[22] is used to model the particle interactions. There are four basic types of interaction sites in the MARTINI force field: polar (P), nonpolar (N), apolar (C), and charged (Q); each of them is categorized into subtypes, thus allowing a more realistic description of the chemical structure. Nonbonded interactions between bead types i and j are described by a Lennard-Jones 12-6 potential characterized by a distance σ_{ij} and interaction strength ε_{ij}. In the MARTINI force field, the values of σ_{ij} are set to 0.47 nm for particle types representing approximately 4 heavy atoms, and 0.43 nm for smaller particles representing 2−3 atoms, including those in rings. For interaction between smaller particles, the ε_{ij} are scaled to 75% with respect to normal particles, and the bead types are renamed by adding the prefix "S". The $C_{12}E_5$ systems require three types of interaction sites: C_1 for the hydrocarbon fragments, SP_2 for the hydroxyl group, and SN_a for the

ethylene glycol residues. The chosen mapping scheme of $C_{12}E_5$ is represented in Figure 1. Because a monomer of PEO includes 3 heavy atoms (COC), the "S" type bead is used. However, in a previous parametrization of PEO polymers,[24] it is found that the self-interaction between PEO beads is not strong enough when using the N_a level. Thus, the PEO bead is made more attractive to itself than expected on the basis of the small-molecule-parametrization of the standard MARTINI force field. In effect, as far as the PEO−PEO interaction is concerned, the PEO bead is treated as a SN_{da} type. Particles are linked together by a stiff harmonic potential with spring constant k_{bond} = 17 000 kJ mol^{-1} nm^{-2} and length b = 0.33 nm for the beads of the head and k_{bond} = 1250 kJ mol^{-1} nm^{-2} and length b = 0.47 nm for the tail part. For the bond connecting the two parts, k_{bond} = 1250 kJ mol^{-1} nm^{-2} and length b = 0.37 nm is used. The solvent is explicit CG water, each bead comprising four water molecules. The C12E5_CG.itp file for Gromacs containing all of the information for the topology of $C_{12}E_5$ and the parameters used in this study is included in the Supporting Information. Further example input files are available from http://cgmartini.nl.

Validation With Respect To All-Atom Simulations. For validation of the CG parameters, two sets of simulations (CG-MD and all-atom, AA-MD) of dimers of the surfactants under study are performed. To this end, two $C_{12}E_5$ molecules are randomly positioned in a cubic box with explicit solvent, in a NPT ensemble with P = 1 bar and T = 293 K. The Berendsen method is applied for the temperature and pressure couplings. First, a CG-MD simulation with length 1 μs is carried out to assess the mutual orientation of the surfactants. A number of sufficiently populated alignments were used as initial geometries for subsequent AA-MD simulations with length 10 ns, using a time-step of 2 fs. For the AA simulations, the AMBER 99[32] force field are utilized, upgraded with our parameters for the ethyleneglycol groups.[33] The C12E5_AA.itp file for Gromacs containing all of the information for the topology of $C_{12}E_5$ and the parameters used in this study is included in the Supporting Information. The same simulation conditions as for the CG models are applied. TIP4P[34] is the solvent model applied for the AA calculations. The particle mesh Ewald (PME) algorithm[35] is employed for evaluating the long-range electrostatic terms. The van der Waals interactions are truncated at a spherical cutoff of 1.2 nm using a switching function. Cluster analysis of the CG-MD and AA-MD trajectories (Figure 2) reveals analogous alignments and molecular conformations. The probability distribution of the similar clusters is also comparable.

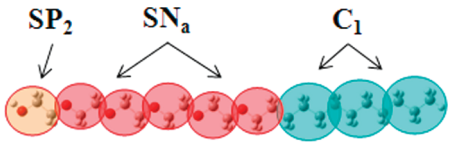

Figure 1. Mapping between the all-atom structure and the CG beads for $C_{12}E_5$. The hydroxyl group at the head is modeled as SP_2 particle (yellow), the poly ethylene glycol unit by five SN_a particles (red), and the aliphatic tail by three C_1 particles (blue).

Figure 3A,B compares the end-to-end distance distributions for the two molecules in the $C_{12}E_5$ dimers. The overall agreement of the CG and all-atom results is good. The plots reveal the similarity of the obtained end-to-end distance for the selected conformation, with one of the molecules (molecule 2) being more extended than the other (molecule 1).

The conformation and mutual orientation of the molecules in the dimers are further analyzed on the basis of the two dihedral angles $tail_1-head_1-head_2-tail_2$ and $head_1-tail_1-tail_2-head_2$. Each cluster is characterized by a specific distribution of these angles, and we use this pattern as a fingerprint for structural similarity of the dimers in AA and CG simulations. In Figure 3C,D are presented the plots for the probability distributions of these dihedral angles for cluster 1 obtained from the cluster analysis (Figure 2). For the $tail_1-head_1-head_2-tail_2$ dihedral shown in Figure 3C, for example, the most typical value of the angle is about 30°, but all other values are populated as well. A preference for angles in the interval −75° to 75° is observed, indicating that the tails do not tend to adopt an antiparallel orientation but rather align at a small angle. The profile for the $head_1-tail_1-tail_2-head_2$ dihedral (Figure 3D) has no clear maxima, but angles around ±120° are predominantly populated. Very similar profiles are obtained for the CG and all-atoms models, confirming the structural similarity of the two approaches for the most populated dimeric aggregate.

Together, these results demonstrate the reliability of the CG parameters used in this study.

RESULTS AND DISCUSSION

Self-Assembly Pathway Depends on Surfactant Concentration. The micellization mechanism in the most diluted and concentrated aqueous solutions of $C_{12}E_5$ is illustrated by snapshots from the trajectories of systems 1 and 4, containing 160 and 1000 surfactant molecules, respectively (Figure 4). The evolution of the number of clusters and of their average size during the simulation is shown in Figure 5. It is assumed that two molecules belong to the same cluster if the distance between the centers of mass (COM) of their tails is shorter than a cutoff. The value 0.5 nm is adopted for this cutoff, being shorter than the distance to the first minimum in the radial distribution function of the tails (Figure S1). The two systems show dissimilar behavior during the simulation. In system 1, the self-assembly of the surfactants into spherical micelles proceeds within ca. 400 ns; the number of clusters and their average sizes remain essentially constant thereafter (Figure 5A,C). System 4 follows a different evolution

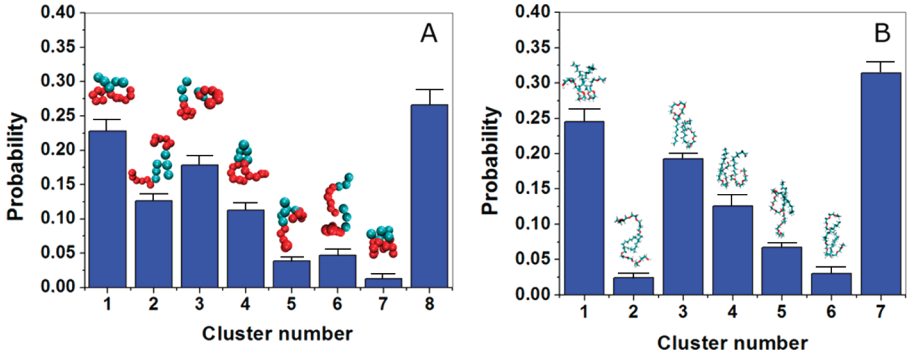

Figure 2. Cluster analysis of the CG-MD (A) and AA-MD (B) trajectories of $C_{12}E_5$ dimers. Representative snapshots of the dimeric alignment are shown for each cluster. Clusters 8 from CG-MD and 7 from AA-MD correspond to structures where the two molecules diverge.

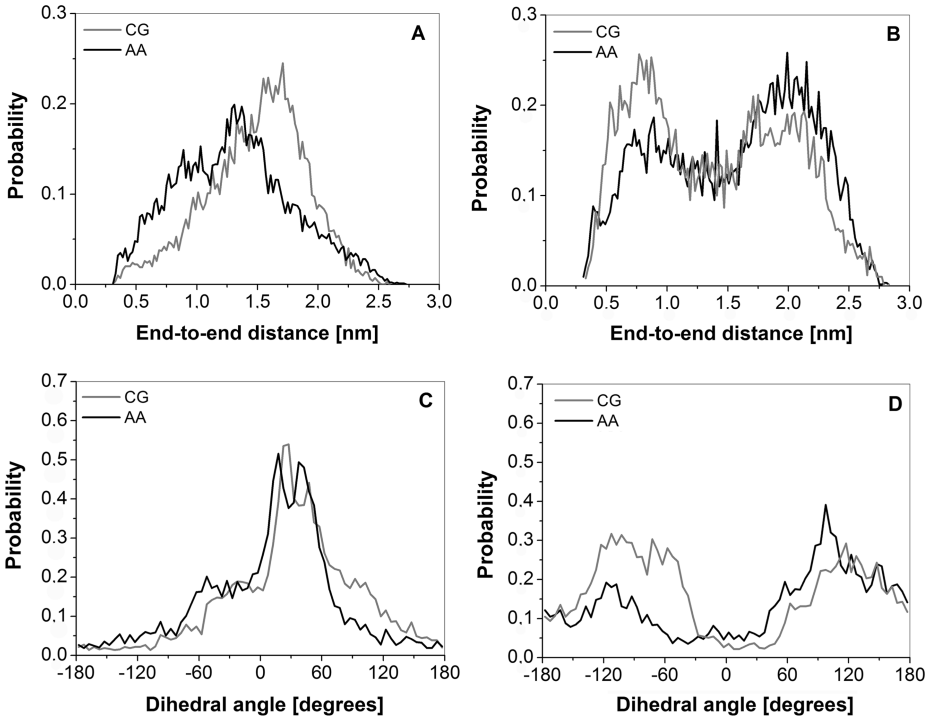

Figure 3. Probability distributions of end-to-end distances for molecule 1 (A) and molecule 2 (B) and probability distributions of the dihedral angles $tail_1-head_1-head_2-tail_2$ (C) and $head_1-tail_1-tail_2-head_2$ (D) of $C_{12}E_5$ dimers from all-atom and CG simulations.

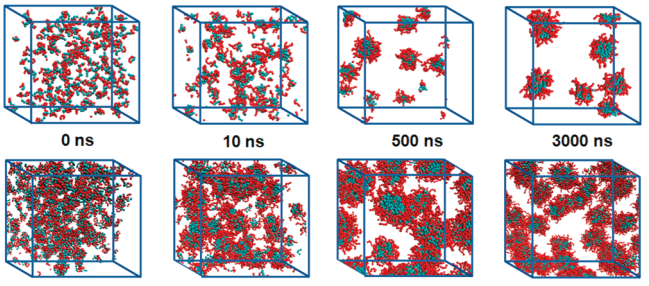

Figure 4. Snapshots of the micelle formation processes for $C_{12}E_5$ in diluted solution with 160 surfactants at χ = 0.13 (upper panel) and concentrated systems with 1000 surfactants at χ = 0.41 (lower panel).

pathway (Figure 5B,D). The initially formed clusters gradually grow in size at the expense of the monomers from the solution. Further extension of the size (after about 1 μs) takes place through fusion of smaller micelles. The model system 2 with 360 surfactants behaves in a fashion similar to system 1, while the more concentrated system 3 with 780 surfactants is much like system 4 (Figure S2). Increase of the surfactant molar fraction leads to significantly higher (by a factor of 2−3) average aggregation numbers. In contrast to the spherical shape of the micelles formed in the more diluted systems, in the denser systems the shape of the aggregates becomes rod-like (see below). In system 1, the most populated cluster at the end of the trajectory is at aggregation numbers between 50 and 60 (see inset in Figure 5A). The average aggregation number (N_{agg}) is 54 ± 1, which is in agreement with the theoretically predicted value of 55 by the SCMF theory[36] for this type of surfactant at low concentration (0.15 mol %). No experimental measurements of the aggregation number around 0.15 mol fraction are known to the authors. In system 4, several well-defined maxima corresponding to various N_{agg} are discernible in the size distribution (inset Figure 5B). The most populated at the end of the simulation is the one with aggregation numbers around 140, which agrees well with the experimentally determined value of 156.[37] However, clusters of sizes ranging between 40 and 120 are still present. Such multitude of populated cluster sizes implies polydispersity of the solution, which is also in accordance with experimental observations.[38] Note that it is still possible that these smaller clusters merge into larger clusters on time scales exceeding the time scale of the simulations (3 μs).

Structural Characterization of Small Micelles. Because the first two stages of micelle formation in $C_{12}E_5$ solutions seem to be concentration independent, deeper knowledge of early micelles characteristics can shed light on their structure at the molecular level and their application-oriented properties. The initial and the final structures of the simulated small micelles (systems 5−8 from Table 1) of $C_{12}E_5$ molecules in explicit water are presented in Figure 6.

Figure 6 contains also larger micelles built of 100 and 120 $C_{12}E_5$ molecules (systems 9, 10 from Table 1). Within the first 200 ns of the trajectory, these larger micelles split into two smaller micelles of aggregation numbers 52 and 48 for 100 $C_{12}E_5$, and 53 and 54 for 120 $C_{12}E_5$ (the remaining surfactants stay as monomers). This is an expected result, bearing in mind that micelles of a size around 50−60 are the stable aggregates in diluted solutions (cf., Figure 5A). These two systems are excluded from further analysis and discussion.

To characterize the overall size and shape of the micelles, we computed a number of structural properties, the radius of gyration R_g, the ratio of principal moments of inertia I_i/I_j, and the relative shape anisotropy K^2. The results are summarized in Table 2. Concerning R_g, our results point at the expected increase of micelle size with aggregation number. The ratios of the average

dx.doi.org/10.1021/la203055t |*Langmuir* 2011, 27, 14071–14077

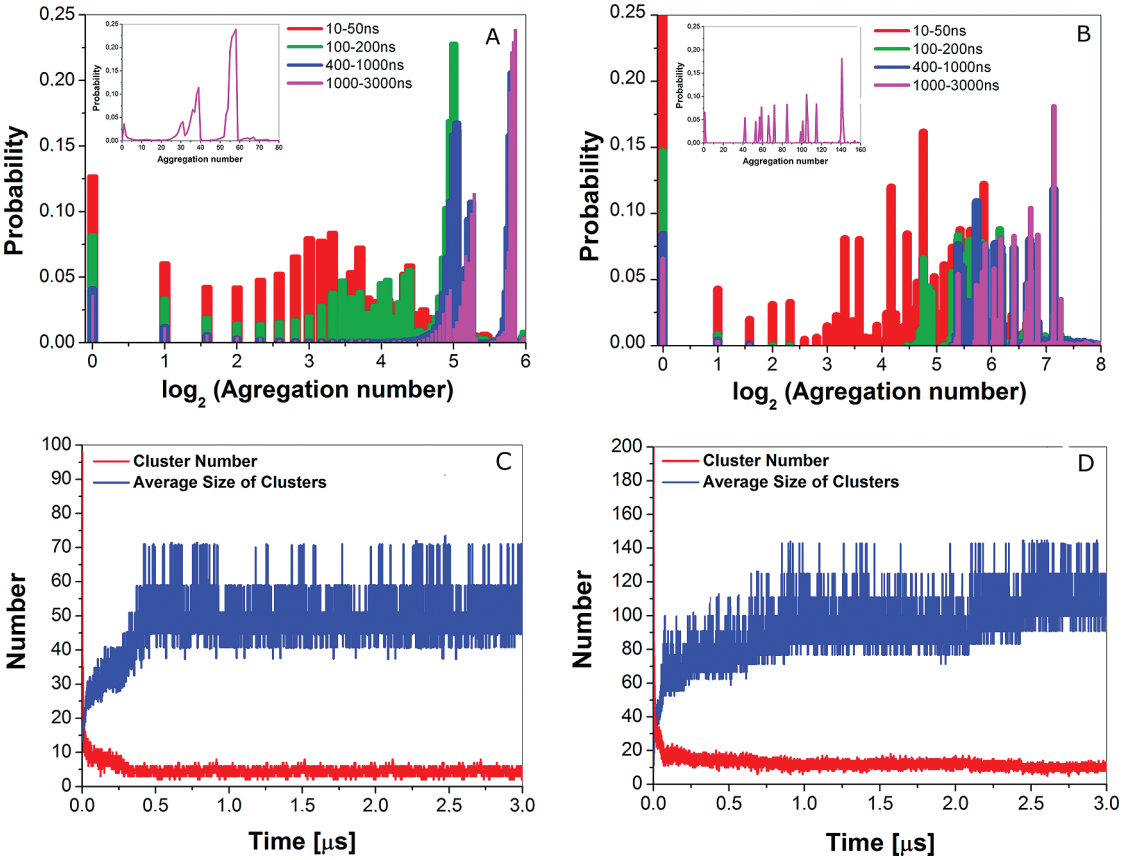

Figure 5. Evolution of cluster size distribution (A,B) and cluster number (C,D) for $C_{12}E_5$ in diluted system with 160 surfactants at $\chi = 0.13$ (A,C) and concentrated system with 1000 surfactants at $\chi = 0.41$ (B,D).

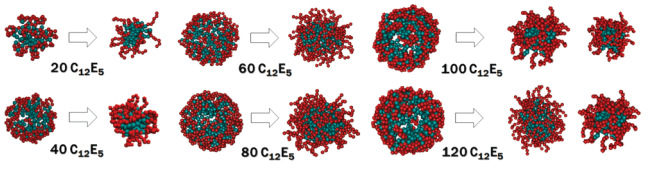

Figure 6. Initial and final micelle shapes of prebuilt micelles of sizes varying between 20 and 120 surfactants.

moments of inertia for the micelles with different size are close to 1, which indicates an almost spherical shape. Deviation from sphericity is moderate and grows with size. Another criterion is the relative shape anisotropy K^2.[39] A linear array of skeletal atoms is characterized with $K^2 = 1$, whereas a molecule with ideal spherical symmetry features $K^2 = 0$. The results confirm the quasi-spherical shape of the micelles for aggregation numbers $\leq$80. This is also evident from the snapshots shown in Figure 4.

The internal structure of the micelle is analyzed by means of radial distribution functions (RDFs). Figure 7 provides an overview of the RDFs of selected components of the micelles and water as a function of their distance from the center of mass of the entire micelle. The surfactant distributions are subdivided into RDFs of heads and tails. The surfactant distributions are Gaussians broadening with the increase of micellar size. Upon growth of the micelles, the hydrophilic heads become less hydrated, pointing to a better shielding of the hydrophobic core of the micelle. To characterize the micelle interior, the RDFs of the tails are further separated into tail fragments (Figure 7, lower panels). Notable is the overlap in density of terminal tail fragments (C3 beads) with the head groups, indicative of rather disordered tail conformations with significant backfolding. The organization of the tail fragments does not seem to depend much on micellar size, however.

Sphere-to-Rod Transition for Micelles of Increasing Size. As alluded to above, upon increasing the surfactant concentration the shape of the micelle changes from spherical to rod-like. To quantify this transition, we determined also the relative shape anisotropy for stable micelles extracted from the self-assembly simulations. For micelles with sizes <80, the calculated values are similar to those presented in Table 2 for the preformed micelles. However, for larger micelles observed at higher concentrations, such analysis cannot be performed as these micelles spontaneously split (cf., Figure 6). All values are combined in Figure 8. For $N_{agg} \leq 80$, the shape anisotropy remains close to zero corresponding to spherically shaped aggregates. For larger micelles, however, the value of K^2 becomes much larger, pointing at an anisotropic shape. Visual inspection (see snapshots in Figure 4) shows that the micelles become rod-like. The transition zone between spherical and rod-like micelle is from $N_{agg} = 80$ to $N_{agg} = 100$. Increasing the aggregation size beyond $N_{agg} \approx 100$ leads to a further increase in shape anisotropy, reflecting extension of the micelles into worm-like aggregates.

To compare to experimental measures, the effective radius of a micelle, R, can be calculated from R_g according to the relation:[40] $R_g^2 = 3R^2/5$. Consequently, for the micelles of $N_{agg} = 60$, $R_g = 1.9$ nm

dx.doi.org/10.1021/la203055t |*Langmuir* 2011, 27, 14071–14077

Table 2. Structural Properties: Radius of Gyration R_g, Ratio of Principal Moments of Inertia I_i/I_j, and Relative Shape Anisotropy K^2 with the Respective Standard Deviations of These Values for Micelles Containing Different Number of Surfactants, N_{sur}[a]

system	N_{sur}	R_g [nm]	I_1/I_2	I_1/I_3	I_2/I_3	K^2
5	20	1.41 ± 0.03	0.98 ± 0.01	0.76 ± 0.01	0.90 ± 0.01	0.006 ± 0.0003
6	40	1.69 ± 0.02	0.89 ± 0.05	0.81 ± 0.05	0.92 ± 0.02	0.003 ± 0.0001
7	60	1.90 ± 0.02	0.88 ± 0.07	0.81 ± 0.09	0.92 ± 0.03	0.004 ± 0.0001
8	80	2.07 ± 0.03	0.85 ± 0.05	0.78 ± 0.09	0.92 ± 0.06	0.005 ± 0.0002

[a] Standard errors are smaller than the last digit listed.

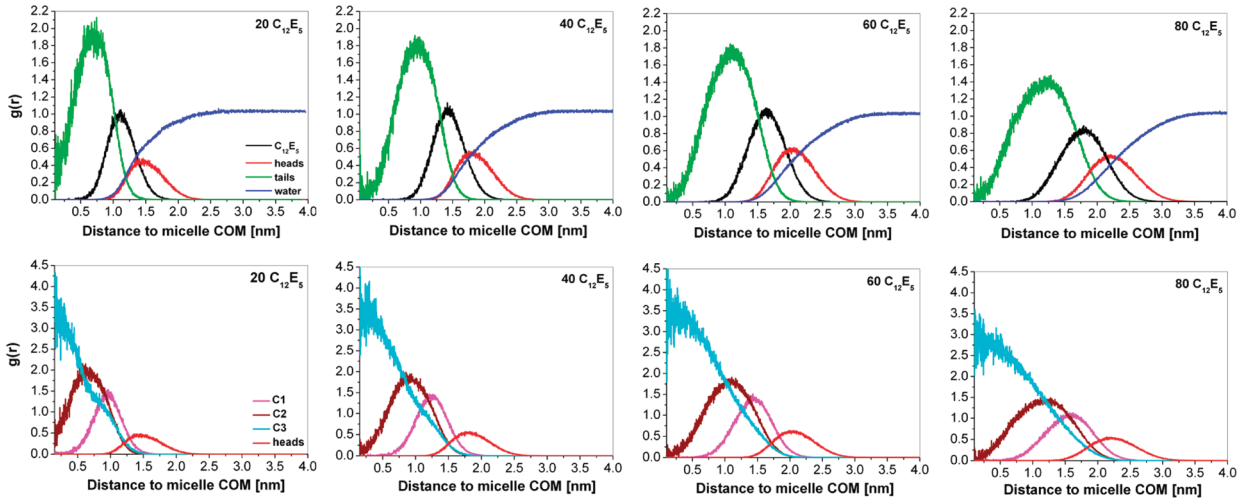

Figure 7. Radial distribution functions $g(r)$ for micelles increasing in size, from 20 (left) to 80 (right) $C_{12}E_5$ surfactants. Upper panels: RDFs divided into water, surfactants ($C_{12}E_5$), heads (SP_2 and SN_a beads, cf., Figure 1), and tails (C_1, C_2, and C_3 beads) contributions with respect to the center-of-mass (COM) of the micelle. Lower panels: RDFs separated for the three tail fragments C_1, C_2, and C_3 (terminal bead).

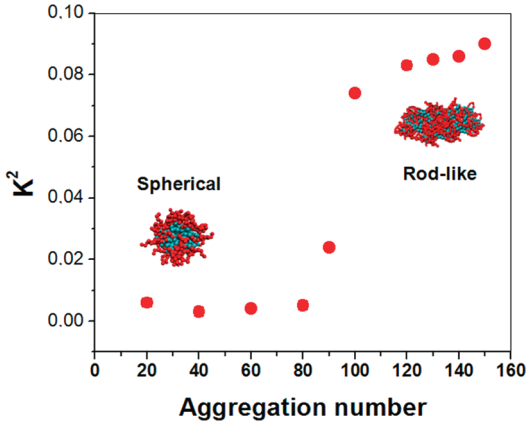

Figure 8. Relative shape anisotropy K^2 against aggregation number of the $C_{12}E_5$ micelles.

and R is 2.5 nm, while for N_{agg} = 150, R_g = 16.1 nm and R = 20.8 nm. These results correspond reasonably to the experimental values of the hydrodynamic radius (R_h) obtained from gel filtration chromatographic study of $C_{12}E_5$ solutions for two sizes of observed micelles: small, R_h = 5 nm, and large, R_h = 30 nm.[33] It is worth noting here that R_h includes both solvent (hydro) and shape (dynamic) effects in the experiment and is typically larger than the theoretically calculated radius based on the radius of gyration.

CONCLUSIONS AND OUTLOOK

The self-organization of $C_{12}E_5$ in aqueous solution is simulated at a coarse-grained level of description. The size and aggregation numbers of the aggregates formed are found in good agreement with the available experimental data. Spherical micelles are formed at the nanosecond scale, growing in size and deviating slightly from sphericity. An increase of concentration is causing a sphere-to-rod transition, with self-assembly slowing down to the microsecond scale due to micelle splitting and fusion events. The critical aggregation number for the sphere-to-rod transition is observed around 90, based on analysis of the shape anisotropy. Further characterization of the internal structure of the micelles reveals a strongly disordered micelle interior that is better shielded from water for increasing micelle size.

Micelles with aggregation number 40−80 are long-living in aqueous solutions of low surfactant concentration, which makes them appropriate for encapsulation and transport of hydrophobic agents. It is known from experiment that $C_{12}E_5$ is useful as a model drug delivery system. Balogh and Pedersen[41] have investigated with small-angle X-ray scattering the effect of adding a drug (lidocaine) to such a system, and they found that about two-thirds of the drug was loaded in the surfactant micelle. Preliminary simulations of a model hydrophobic agent loaded in a micelle containing 60 surfactants revealed a consistent picture. On the other hand, the results of our ongoing theoretical investigations on the series $C_{12}E_n$ (n = 3−5) indicate that the applicability for practical use as nanotransporter enhances with

augmentation of the headgroup size. We expect that the next compounds in the series with n = 6−8 will exhibit more promising behavior as drug delivery systems.

■ ASSOCIATED CONTENT

Supporting Information. Input files (*.itp) for CG and AA simulations of $C_{12}E_5$; Figure S1, RDF of the distance between tail−tail COM in system 1; and Figure S2, evolution of cluster size distribution (A,B) and cluster number (C,D) for $C_{12}E_5$ in diluted system with 360 surfactants at χ = 0.19 (A,C) and concentrated system with 780 surfactants at χ = 0.33 (B,D). This material is available free of charge via the Internet at http://pubs.acs.org.

■ AUTHOR INFORMATION

Corresponding Author

*Tel.: ++359-2-8161374. Fax: ++359-2-962-54-38. E-mail: tadjer@chem.uni-sofia.bg.

■ ACKNOWLEDGMENT

The work has been performed under the Project HPC-EUROPA 2 (project number: 393), with the support of the European Community - Research Infrastructure Action under the FP8 "Structuring the European Research Area", and Projects DO-02-256/2008 and DCVP-02-2/2009 of NSF-Bulgaria. Dr. Anela Ivanova is acknowledged for helpful discussions.

■ REFERENCES

(1) Gelbart, W.; Ben-Shaul, A.; Roux, D. *Micelles: Membranes, Microemulsions and Monolayers*; Springer-Verlag: New York, 1994.
(2) Israelachvili, J. *Intermolecular and Surface Forces*, 2nd ed.; Academic: London, 1992.
(3) Rosen, M. *Surfactants and Interfacial Phenomena*, 2nd ed.; Wiley: New York, 1989.
(4) Sharma, K.; Patil, S.; Rakshit, A. *J. Phys. Chem. B* **2004**, *108*, 12804.
(5) Bernheim-Groswasser, A.; Wachtel, E.; Talmon, Y. *Langmuir* **2000**, *16*, 4131.
(6) Arabadzhieva, D.; Tchoukov, P.; Mileva, E.; Miller, R.; Soklev, B. *Ukr. J. Phys.* **2011**, *56*, 2071.
(7) Glatter, O.; Fritz, G.; Lindner, H.; Brunner-Popela, J.; Mittelbach, R.; Strey, R.; Egelhaaf, S. *Langmuir* **2000**, *16*, 8692.
(8) Drummond, C. J.; Warr, G. G.; Grieser, F.; Evans, D. F.; Ninham, B. W. *J. Phys. Chem.* **1985**, *89*, 2103.
(9) Ben-Shaul, A.; May, S. *J. Phys. Chem. B* **2001**, *105*, 630.
(10) Daful, A. G.; Baulin, V. A.; Avalos, J. B.; Mackie, A. D. *J. Phys. Chem. B* **2011**, *115*, 3434.
(11) Puvvada, S.; Blankschtein, D. *J. Chem. Phys.* **1990**, *92*, 3710.
(12) Sterpone, F.; Briganti, G.; Pierleoni, C. *Langmuir* **2001**, *17*, 5103.
(13) Allen, R.; Bandyopadhyay, S.; Klein, M. L. *Langmuir* **2000**, *16*, 10547.
(14) Sammalkorpi, M.; Karttunen, M.; Haataja, M. *J. Phys. Chem. B* **2007**, *111*, 11722.
(15) Marrink, S. J.; Tieleman, D. P.; Mark, A. E. *J. Phys. Chem. B* **2000**, *104*, 12165.
(16) Marrink, S. J.; Mark, A. E. *Biochemistry* **2002**, *41*, 5375.
(17) Jorge, M. *Langmuir* **2008**, *24*, 5714.
(18) Loverde, S. M.; Ortiz, V.; Kamien, R. D.; Kleinaf, M. L.; Discher, D. L. *Soft Matter* **2010**, *6*, 1419.
(19) Gao, J.; Li, S.; Zhang, X.; Wang, W. *Phys. Chem. Chem. Phys.* **2010**, *12*, 3219.
(20) Pool, R.; Bolhuis, P. G. *Phys. Rev. Lett.* **2006**, *97*, 018302.
(21) Shinoda, W.; DeVane, R.; Klein, M. L. *Soft Matter* **2008**, *4*, 2454.
(22) Marrink, S.-J.; de Vries, A. H.; Mark, A. E. *J. Phys. Chem. B* **2004**, *108*, 750.
(23) Marrink, S.-J.; Risselada, H. J.; Yefimov, S.; Tieleman, D. P.; de Vries, A. H. *J. Phys. Chem. B* **2007**, *111*, 7812.
(24) Lee, H.; de Vries, A. H.; Marrink, S.-J.; Pastor, R. W. *J. Phys. Chem. B* **2009**, *113*, 13186.
(25) Sangwai, V. A.; Sureshkumar, R. *Langmuir* **2011**, *11*, 6628.
(26) Sanders, S. A.; Panagiotopoulos, A. Z. *J. Chem. Phys.* **2010**, *132*, 114902.
(27) Lee, H.; Pastor, R. W. *J. Phys. Chem. B* **2011**, *115*, 7830.
(28) Mitchell, D. J.; Tiddy, G. J. T.; Waring, L.; Bostock, T.; McDonald, M. P. *J. Chem. Soc., Faraday Trans. 1* **1983**, *79*, 975.
(29) Bernheim-Groswasser, A.; Wachtel, E.; Talmon, Y. *Langmuir* **2000**, *16*, 4131.
(30) Hess, B.; Kutzner, C.; Spoel, D. v. d.; Lindahl, E. *J. Chem. Theory Comput.* **2008**, *4*, 435.
(31) Berendsen, H. J. C.; Postma, J. P. M.; DiNola, A.; Haak, J. R. *J. Chem. Phys.* **1984**, *81*, 3684.
(32) Wang, J.; Cieplak, P.; Kollman, P. A. *J. Comput. Chem.* **2000**, *21*, 1049.
(33) Velinova, M.; Tsoneva, Y.; Shushkov, Ph.; Ivanova, A.; Tadjer, A. *Prog. Theor. Chem. Phys.* **2011**, *Chapter 26*, 463.
(34) Jorgensen, W. L.; Madura, J. D. *Mol. Phys.* **1985**, *56*, 1381.
(35) Essmann, U.; Perera, L.; Berkowitz, M. L.; Darden, T.; Lee, H.; Pedersen, L. G. *J. Chem. Phys.* **1995**, *103*, 8577.
(36) Al-Anbera, Z.; Bonet, J.; Avalos, M.; Floriano, A.; Mackie, D. A. *J. Chem. Phys.* **2003**, *118*, 3816.
(37) Kwon, Y. S.; Kim, W. M. *Langmuir* **2001**, *17*, 8016.
(38) Funasaki, N.; Hada, S.; Neya, A. *Bull. Chem. Soc. Jpn.* **1989**, *62*, 2485.
(39) Theodorou, D. N.; Suter, U. W. *Macromolecules* **1985**, *18*, 1206.
(40) Rubinstein, M.; Colby, R. H. *Polymer Physics*, 1st ed.; Oxford University Press: New York, 2003.
(41) Balogh, J.; Pedersen, J. S. *Prog. Colloid Polym. Sci.* **2008**, *135*, 101.